Journal of Systems Engineering and Electronics
Vol. PP, No. 99, October 2023, pp.1 – 11

Coarse-fine joint target parameter estimation method based on AN-RSC in OFDM passive radar

WANG Chujun, WAN Xianrong*, YI Jianxin, and CHENG Feng

School of Electronic Information, Wuhan University, Wuhan 430072, China

Abstract: In this paper, we study the accuracy of delay-Doppler parameter estimation of targets in a passive radar using orthogonal frequency division multiplexing (OFDM) signal. A coarse-fine joint estimation method is proposed to achieve better estimation accuracy of target parameters without excessive computational burden. Firstly, the modulation symbol domain (MSD) method is used to roughly estimate the delay and Doppler of targets. Then, to obtain high-precision Doppler estimation, the atomic norm (AN) based on the multiple measurement vectors (MMV) model (MMV-AN) is used to manifest the signal sparsity in the continuous Doppler domain. At the same time, a reference signal compensation (RSC) method is presented to obtain high-precision delay estimation. Simulation results based on the OFDM signal show that the coarse-fine joint estimation method based on AN-RSC can obtain a more accurate estimation of target parameters compared with other algorithms. In addition, the proposed method also possesses computational advantages compared with the joint parameter estimation.

Keywords: passive radar, orthogonal frequency division multiplexing (OFDM) signal, atomic norm (AN), parameter estimation.

DOI: 10.23919/JSEE.2023.000100

1. Introduction

Passive radar, which utilizes the existing illuminators of opportunity to achieve target detection and tracking, has attracted increasing interest in recent years [1−3]. In addition, with the rapid popularization of digital broadcasting using orthogonal frequency division multiplexing (OFDM) modulation, such as digital audio broadcasting (DAB) [4], digital video broadcasting-terrestrial (DVB-T) [5], and digital terrestrial multimedia broadcasting (DTMB) [6], some novel estimations of target parameters are designed that make full use of the two-dimensional (2D) structure of the OFDM signal. In [7], a modulation symbol domain (MSD) method was proposed to estimate the delay and Doppler of the targets. Because the estimation is less susceptible to imperfect autocorrelation characteristics of baseband signals, this method provides a significantly higher peak to sidelobe ratio. However, the delay and Doppler resolution of the MSD are limited by signal bandwidth and accumulation time, respectively. To cope with this limitation, spatial spectrum estimation algorithms or sparse methods can be used in target parameter estimation, but they may incur higher computational complexity [8,9].

The multiple signal classification (MUSIC) algorithm, a typical subspace classification method, is widely used for target parameter estimation due to its good resolution and accuracy [10]. However, the estimation accuracy of MUSIC algorithm is susceptible to the signal to noise ratio (SNR), which leads to poor estimation performance in noisy environments. With the development of sparse signal representation and later the compressed sensing (CS) theory [11−13], sparse methods have been developed for improving the accuracy of parameter estimation [14]. When the CS algorithm has been considered in range Dopper (RD) map generation, the dictionary consists of the template signals with discrete delays and Doppler frequencies [15,16], and therefore the delays and frequencies of targets are assumed to be distributed on some fixed delay-frequency grids [17]. However, since the targets and clutter are often determined by parameters (delays and Doppler frequencies) in a continuous domain, the discretization tends to lead to model mismatches and poor recovery performance [18].

In order to address the grid mismatch problem caused by traditional sparse methods, a mathematical theory of continuous sparse recovery was proposed to achieve super-resolution [19,20]. Zheng et al. [21] used the atomic norm (AN) constraint to formulate the sparsity of signals in the delay-Doppler plane, and the results have

Manuscript received March 17, 2022.
*Corresponding author.
This work was supported by the National Natural Science Foundation of China (61931015; 62071335), the Technological Innovation Project of Hubei Province of China (2019AAA061), and the Natural Science Foundation of Hubei Province of China (2021CFA002).

better performance compared with the existing high-resolution methods based on CS and 2D-MUSIC algorithms. However, if AN is directly applied to delay-Doppler parameter estimation with a long integration time and high sampling frequency, although the alternating direction method of multipliers (ADMM) [22] was used in [21] to effectively solve the semidefinite program (SDP), it still needs a lot of computation and may hinder the real-time application for it involves convex optimization. To further reduce the computational complexity of the algorithm， another approach is to utilize a series of one-dimensional (1D) searches that alternate between optimizations on one variable while keeping the other variable fixed, which better achieves 2D joint estimation without the heavy computational burden [17,23].

Based on the methods above, we propose a new parameter estimation method for OFDM-based passive radar. A coarse-fine joint estimation method is presented, in which only a few batches are selected for parameter estimation to reduce calculations. Firstly, the method proposed in [7] is used to roughly estimate the delay and Doppler frequency of targets. Then the AN and reference signal compensation (RSC) methods are used in the Doppler domain and delay domain, respectively, and the generated Topeplitz matrix of AN no longer needs huge storage space. In the Doppler dimension, the AN based on the multiple measurement vectors (MMV) [24] model (MMV-AN) is used to improve the processing ability. In the delay dimension, the RSC is presented to overcome the loss of SNR caused by the block processing of the signal, which can easily achieve the accuracy and robustness of delay estimation.

The remainder of the paper is organized as follows. In Section 2, the passive radar signal model in the subcarrier domain is described. In Section 3, a new coarse-fine joint parameter estimation AN-RSC method for OFDM passive radar is proposed. In Section 4, the effectiveness of the proposed method is presented via numerical simulation and computational complexity analysis. Finally, conclusions are drawn in Section 5.

2. Signal model and problem representation

We study the passive radar system utilizing OFDM signals, which can be viewed as parallel streams of multiple single-carrier signals with orthogonal carrier waveforms, each modulated using different transmission data [7]. The transmitted data is divided into multiple OFDM symbols. The duration of each OFDM symbol is $T_{\mathrm{S}}=T+T_{\mathrm{G}}$, which is composed of an elementary symbol duration T and a guard interval duration T_{G}. Assume that there are N_{c} orthogonal subcarriers in each OFDM symbol, and the nth subcarrier frequency is $f_n=n\Delta f$, where $\Delta f=1/T$ is the subcarrier interval. The transmitted signal in the mth OFDM symbol can be modeled as

$$x_m(t)=\sum_{n=0}^{N_{\mathrm{c}}-1}s_m[n]\exp(\mathrm{j}2\pi n\Delta f t)\cdot\xi(t-mT_{\mathrm{S}}),\quad mT_{\mathrm{S}}-T_G\leqslant t\leqslant mT_{\mathrm{S}}+T \tag{1}$$

where $s_m[n]$ $(n=0,1,\cdots,N_{\mathrm{c}}-1;\ m=0,1,\cdots,N_{\mathrm{sym}}-1)$ is complex modulation data with the nth subcarrier of the mth OFDM symbol, and

$$\xi(t)=\begin{cases}1, & t\in[-T_G,T]\\ 0, & \text{otherwise}\end{cases}. \tag{2}$$

A typical passive radar includes two channels, a reference channel and a surveillance channel. In OFDM-based passive radar, on the surveillance side, suppose down-conversion has been carried out, and only baseband signals are considered below. The received signals contain direct path interference, target echoes, multipath signals, and noise. Assume there are K paths, it can be modeled as

$$\begin{aligned}y(t)=&\sum_{m=0}^{N_{\mathrm{sym}}-1}\sum_{k=1}^{K}A_k\exp(\mathrm{j}2\pi f_k t)\cdot\\ &x_m(t-\tau_k)+\omega(t)\approx\\ &\sum_{m=0}^{N_{\mathrm{sym}}-1}\sum_{k=1}^{K}A_k\exp(\mathrm{j}2\pi f_k mT_{\mathrm{s}})\cdot\\ &x_m(t-\tau_k)+\omega(t)\end{aligned} \tag{3}$$

where τ_k and f_k denote as the delay and Doppler shift of the kth path, respectively; A_k is an attenuation coefficient containing path loss, reflection and processing gains; $\omega(t)$ is additive noise. The approximation in (3) is derived from the constant phase rotation approximation within an OFDM block [21].

Performe Fourier transform on the surveillance signal of (3) in the mth OFDM symbol, then the signal in the nth subcarrier can be expressed as

$$\begin{aligned}r_m[n]=&\sum_{k=1}^{K}\alpha_k s_m[n]\exp(\mathrm{j}2\pi f_k mT_{\mathrm{s}})\cdot\\ &\exp(-\mathrm{j}2\pi f_n\tau_k)+v_m[n]\end{aligned} \tag{4}$$

where α_k is the complex amplitude of the kth target, $\alpha_k=A_kT$, and $v_m[n]$ is a complex Gaussian variable with zero mean and variance δ^2.

In order to implement a processor for the estimation of delay and Doppler frequency, the transmitted information has to be removed from the surveillance channel firstly. In OFDM-based passive radar, the reference signal includes a direct path signal and multipath signals, and the clean reference signal $x_{\mathrm{ref}}=s_m[n]$ can be obtained by reconstruction [25]. Therefore, the transmitted signal

can be effectively removed from the surveillance information symbols by the complex division of elements for low-order modulation schemes such as binary phase shift keying (BPSK) and quadrature phase shift keying (QPSK) [7]. Let $\boldsymbol{D}$ be a new matrix, and its element $D_{n,m}$ is equal to the receiving symbol $r_m[n]$ divided by the reference symbol $x_m[n]$ [26], $\boldsymbol{D}$ is given as

$$\boldsymbol{D}=\begin{bmatrix} D_{0,0} & D_{0,1} & \cdots & D_{0,N_{\mathrm{sym}}-1} \\ D_{1,0} & D_{1,1} & \cdots & D_{1,N_{\mathrm{sym}}-1} \\ \vdots & \vdots & & \vdots \\ D_{N_{\mathrm{c}}-1,0} & D_{N_{\mathrm{c}}-1,1} & \cdots & D_{N_{\mathrm{c}}-1,N_{\mathrm{sym}}-1} \end{bmatrix} \tag{5}$$

where

$$D_{n,m}=r_m[n]/s_m[n]=\sum_{k=1}^{K}\alpha_k\exp(\mathrm{j}2\pi f_k mT)\cdot \exp(-\mathrm{j}2\pi f_n\tau_k)+\varpi_m[n].$$

The problem is to estimate the unknown parameters reflections α_k, delays τ_k, and Doppler shifts f_k of targets in (5).

3. Coarse-fine joint estimation method based on AN-RSC

In this section, a coarse-fine joint estimation method based on AN-RSC is presented to achieve high-precision estimation of Doppler frequency and delay respectively with OFDM-based passive radar data, and the signal processing flow chart can be seen in Fig. 1. There are three main modules: rough estimation of Doppler and delay parameters, precise estimation of Doppler parameters, and precise estimation of delay parameters. First, the rough estimation of the parameters of the interesting targets is conducted by the MSD method. Then, combined with the rough estimation parameters, AN and RSC methods are used to realize the high-precision estimation of Doppler and delay, respectively. The specific operation of each module is as follows.

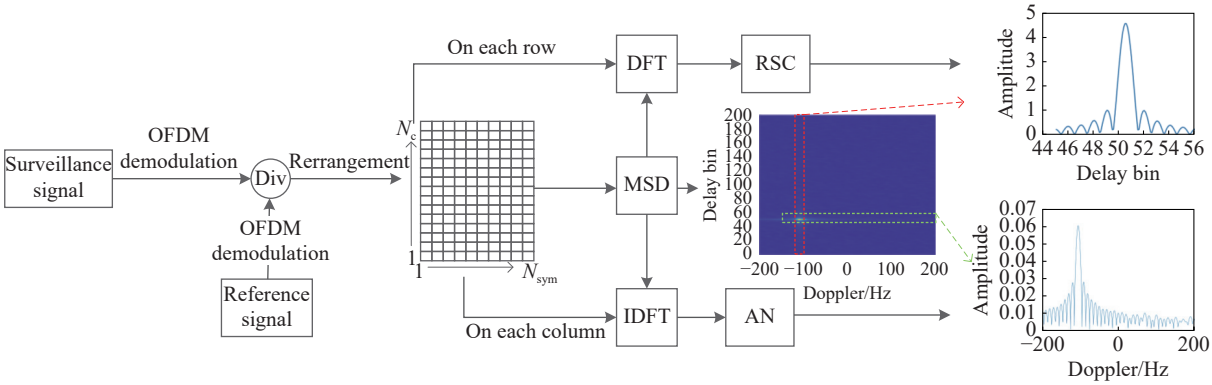

Fig. 1 Flow chart of the estimation of Doppler and delay

3.1 Rough estimation of target parameters

Construct a new sparse matrix $\boldsymbol{X}$ whose non-zero elements x_{τ,f_D} represent reflective targets or clutter, given as

$$x_{\tau,f_D}=\begin{cases}\alpha_k, & \tau=\tau_k; f_D=f_k \\ 0, & \text{otherwise}\end{cases}. \tag{6}$$

Then, (5) can be apporximated as

$$\boldsymbol{D}=\boldsymbol{F}_{N_{\mathrm{c}}}\boldsymbol{X}\boldsymbol{F}_{N_{\mathrm{sym}}}^{\mathrm{H}}+\boldsymbol{\omega} \tag{7}$$

where $\boldsymbol{F}_{N_{\mathrm{c}}}$ and $\boldsymbol{F}_{N_{\mathrm{sym}}}$ denote Fourier transform matrices of different sizes $N_{\mathrm{c}}\times N_{\mathrm{c}}$ and $N_{\mathrm{sym}}\times N_{\mathrm{sym}}$, respectively; $\boldsymbol{\omega}$ is the additive noise matrix; $(\cdot)^{\mathrm{H}}$ represents the conjugate transformation of a matrix. To obtain high precision parameter estimation effectively, the method proposed in [7] is used to estimate the target parameters roughly. For Doppler parameter estimation, a classical spectrum estimation method is used, formally, the inverse discrete Fourier transform (IDFT) is performed for each column of the matrix $\boldsymbol{D}$ in (7), one has

$$\boldsymbol{Y}_1=\boldsymbol{F}_{N_{\mathrm{c}}}^{\mathrm{H}}\boldsymbol{D}=\boldsymbol{F}_{N_{\mathrm{c}}}^{\mathrm{H}}\boldsymbol{F}_{N_{\mathrm{c}}}\boldsymbol{X}\boldsymbol{F}_{N_{\mathrm{sym}}}^{\mathrm{H}}+\boldsymbol{F}_{N_{\mathrm{c}}}^{\mathrm{H}}\boldsymbol{\omega}= \boldsymbol{X}\boldsymbol{F}_{N_{\mathrm{sym}}}^{\mathrm{H}}+\boldsymbol{F}_{N_{\mathrm{c}}}^{\mathrm{H}}\boldsymbol{\omega}. \tag{8}$$

The discrete Fourier transform (DFT) is calculated for every row of the matrix $\boldsymbol{Y}_1$ in (8). The resulting matrix $\boldsymbol{Y}$ in (9) directly represents a 2D RD map:

$$\boldsymbol{Y}=\boldsymbol{Y}_1\boldsymbol{F}_{N_{\mathrm{sym}}}=\boldsymbol{X}+\boldsymbol{F}_{N_{\mathrm{c}}}^{\mathrm{H}}\boldsymbol{\omega}\boldsymbol{F}_{N_{\mathrm{sym}}}=\boldsymbol{X}+\tilde{\boldsymbol{\omega}}. \tag{9}$$

From the RD map given in (9), we can preliminarily obtain the delay and Doppler frequency parameters of the interesting targets expressed as $\boldsymbol{G}_{\tau,f}\in\mathbf{R}^{P\times 2}$, where P represents the total number of the point targets of interest. $\boldsymbol{G}_{\tau,f}(p,\ :)=\left(g_\tau^p,\ g_f^p\right)(p\in[1,P])$ denotes the delay bin g_τ^p and Doppler shift g_f^p of the pth target.

3.2 Doppler parameters estimation

In this subsection, the high-precision estimation of the

Doppler frequency of the interested point target is mainly carried out. The multivariable estimation problem in (7) becomes at most N_{c} parallel univariate estimation process. In (8), the ith row of the matrix $\boldsymbol{Y}_1$ be expressed as

$$y_i = \sum_{k=1}^{K} c_k \exp(\mathrm{j}2\pi f_k m T_{\mathrm{s}}) \in \mathbf{C}^{1\times N_{\mathrm{sym}}} \tag{10}$$

where c_k and $\exp(\mathrm{j}2\pi f_k m T_{\mathrm{s}})$ denote the coefficient and atom corresponding to the kth scattering center respectively, and f_k is the normalized frequency. For (10), the following continuous dictionary set is established:

$$\mathcal{A} = \{\, a(f) : f \in [0,1]\}. \tag{11}$$

Note that the method in [24], the MMV at a single step while the joint processing exploiting in a unified framework can provide a sufficient condition for exact recovery. To facilitate the practical operation, we adopt the method of partial extraction of data, which can be expressed as

$$\boldsymbol{Y}_{1\_\mathrm{sub}} = \boldsymbol{\Psi}_p \boldsymbol{Y}_1 \tag{12}$$

where $\boldsymbol{\Psi}_p \in \mathbf{R}^{P\times N_{\mathrm{c}}}$ denote a partial identity matrix, which is determined by delay bin $\boldsymbol{G}_{\tau,f}(:, 1)$ obtained by (9). Therefore, the MMV-AN for the signal $\boldsymbol{Y}_{1\_\mathrm{sub}} \in \mathbf{C}^{P\times N_{\mathrm{sym}}}$ can be defined as

$$\left\|\boldsymbol{Y}_{1\_\mathrm{sub}}\right\|_{\mathcal{A}} = \inf_{\boldsymbol{c}_p, f_k}\left\{\sum_p \left\|c_p\right\|_2 : \boldsymbol{Y}_{1\_\mathrm{sub}} = \sum_p \boldsymbol{c}_p \boldsymbol{a}(f_{k,p})\right\}. \tag{13}$$

where $\inf\{\cdot\}$ is the infimum

We can recover $\hat{\boldsymbol{Y}}_{1\_\mathrm{sub}}$ using the MMV-AN minimization as follows:

$$\begin{aligned}&\hat{\boldsymbol{Y}}_{1\_\mathrm{sub}} = \arg\min_{\hat{\boldsymbol{Y}}_{1\_\mathrm{sub}}} \left\|\hat{\boldsymbol{Y}}_{1\_\mathrm{sub}}\right\|_{\mathcal{A}}\\ &\text{s.t. } \left\|\hat{\boldsymbol{Y}}_{1\_\mathrm{sub}} - \boldsymbol{Y}_{1\_\mathrm{sub}}\right\|_{\mathrm{F}}^2 \leqslant \varepsilon.\end{aligned} \tag{14}$$

Or, equivalently, the semidefinite program

$$\begin{aligned}&\{\hat{\boldsymbol{Y}}_{1\_\mathrm{sub}}, \boldsymbol{T}(\boldsymbol{u})\} =\\ &\arg\min_{u,\hat{\boldsymbol{Y}}_{1\_\mathrm{sub}}} \frac{\tau}{2}[\mathrm{tr}(\boldsymbol{T}(\boldsymbol{u})) + \mathrm{tr}(\boldsymbol{\Phi})]\\ &\text{s.t.}\begin{bmatrix}\boldsymbol{\Phi} & \hat{\boldsymbol{Y}}_{1\_\mathrm{sub}}\\ (\hat{\boldsymbol{Y}}_{1\_\mathrm{sub}})^{\mathrm{H}} & \boldsymbol{T}(\boldsymbol{u})\end{bmatrix} \succeq 0,\\ &\boldsymbol{\Phi} = \boldsymbol{\Phi}^{\mathrm{H}}, \left\|\hat{\boldsymbol{Y}}_{1\_\mathrm{sub}} - \boldsymbol{Y}_{1\_\mathrm{sub}}\right\|_{\mathrm{F}}^2 \leqslant \varepsilon\end{aligned} \tag{15}$$

where $\tau = 1/\sqrt{N_{\mathrm{sym}}}$ and $\mathrm{tr}(\cdot)$ is the trace of the input matrix; $\boldsymbol{\Phi} \in \mathbf{C}^{P\times P}$ is a Hermitian matrix; $\boldsymbol{u} \in \mathbf{C}^{N_{\mathrm{sym}}}$ and $\boldsymbol{T}(\boldsymbol{u}) \in \mathbf{C}^{N_{\mathrm{sym}}\times N_{\mathrm{sym}}}$ is the Toeplitz matrix of a vector $\boldsymbol{u}$; the notation $\succeq$ indicates that the matrix is positive semi-definite. The problem of the semidefinite program in (15) can be solved by ready-made solvers such as self-dual-minimization (SeDuMi) [27] and SDPT3 [28]. However, these solvers are usually slow when solving large-scale data, so a reasonably efficient algorithm based upon the ADMM is used in this paper. Express our problem in the appropriate ADMM form, then (15) can be rewritten as

$$\begin{aligned}&\{\hat{\boldsymbol{Y}}_{1\_\mathrm{sub}}, \boldsymbol{T}(\boldsymbol{u})\} = \arg\min_{u,\hat{\boldsymbol{Y}}_{1\_\mathrm{sub}}} \frac{1}{2}\left\|\hat{\boldsymbol{Y}}_{1\_\mathrm{sub}} - \boldsymbol{Y}_{1\_\mathrm{sub}}\right\|_{\mathrm{F}}^2 +\\ &\qquad \frac{\tau}{2}[\mathrm{tr}(\boldsymbol{T}(\boldsymbol{u})) + \mathrm{tr}(\boldsymbol{\Phi})]\\ &\text{s.t.}\begin{cases}\boldsymbol{U} = \begin{bmatrix}\boldsymbol{\Phi} & \hat{\boldsymbol{Y}}_{1\_\mathrm{sub}}\\ (\hat{\boldsymbol{Y}}_{1\_\mathrm{sub}})^{\mathrm{H}} & \boldsymbol{T}(\boldsymbol{u}\end{bmatrix} \succeq 0\\ \boldsymbol{\Phi} = \boldsymbol{\Phi}^{\mathrm{H}}\end{cases}.\end{aligned} \tag{16}$$

By dualize the equality constraint by augmented Lagrangian, there are

$$\begin{aligned}&L(\hat{\boldsymbol{Y}}_{1\_\mathrm{sub}}, u, \boldsymbol{\Phi}, \boldsymbol{\Lambda}, \boldsymbol{U}) =\\ &\frac{1}{2}\left\|\hat{\boldsymbol{Y}}_{1\_\mathrm{sub}} - \boldsymbol{Y}_{1\_\mathrm{sub}}\right\|_{\mathrm{F}}^2 + \frac{\tau}{2}[\mathrm{tr}(\boldsymbol{T}(\boldsymbol{u})) + \mathrm{tr}(\boldsymbol{\Phi})] +\\ &\left\langle \boldsymbol{\Lambda}, \boldsymbol{U} - \begin{bmatrix}\boldsymbol{\Phi} & \hat{\boldsymbol{Y}}_{1\_\mathrm{sub}}\\ (\hat{\boldsymbol{Y}}_{1\_\mathrm{sub}})^{\mathrm{H}} & \boldsymbol{T}(\boldsymbol{u})\end{bmatrix}\right\rangle +\\ &\frac{\rho}{2}\left\|\boldsymbol{U} - \begin{bmatrix}\boldsymbol{\Phi} & \hat{\boldsymbol{Y}}_{1\_\mathrm{sub}}\\ (\hat{\boldsymbol{Y}}_{1\_\mathrm{sub}})^{\mathrm{H}} & \boldsymbol{T}(\boldsymbol{u})\end{bmatrix}\right\|_{\mathrm{F}}^2\end{aligned} \tag{17}$$

where the fourth term on the right side of (17) is the penalty term, and ρ is the penalty term coefficient. We set $\rho = 2\delta\sqrt{N_{\mathrm{sym}}\log_2 N_{\mathrm{sym}}}$ and δ is the standard variance of the noise obtained from base statistics without targets in (8). $\boldsymbol{\Phi}$, $\boldsymbol{\Lambda} \in \mathbf{C}^{(P+N_{\mathrm{sym}})\times(P+N_{\mathrm{sym}})}$, and $\boldsymbol{U} \in \mathbf{C}^{(P+N_{\mathrm{sym}})\times(P+N_{\mathrm{sym}})}$ are Hermitian matrices, and

$$\begin{cases}\boldsymbol{\Lambda} = \begin{bmatrix}\boldsymbol{\Lambda}_{P\times P} & \boldsymbol{\Lambda}_{P\times N_{\mathrm{sym}}}\\ \boldsymbol{\Lambda}_{N_{\mathrm{sym}}\times P} & \boldsymbol{\Lambda}_{N_{\mathrm{sym}}\times N_{\mathrm{sym}}}\end{bmatrix}\\ \boldsymbol{U} = \begin{bmatrix}\boldsymbol{U}_{P\times P} & \boldsymbol{U}_{P\times N_{\mathrm{sym}}}\\ \boldsymbol{U}_{N_{\mathrm{sym}}\times P} & \boldsymbol{U}_{N_{\mathrm{sym}}\times N_{\mathrm{sym}}}\end{bmatrix}\end{cases}. \tag{18}$$

The ADMM [29] contains the following update steps:

$$\begin{aligned}&(\hat{\boldsymbol{Y}}_{1\_\mathrm{sub}}^{t+1}, \boldsymbol{u}^{t+1}, \boldsymbol{\Phi}^{t+1}) =\\ &\arg\min_{\hat{\boldsymbol{Y}}_{1\_\mathrm{sub}}, \boldsymbol{u}, \boldsymbol{\Phi}} L(\hat{\boldsymbol{Y}}_{1\_\mathrm{sub}}, \boldsymbol{u}, \boldsymbol{\Phi}, \boldsymbol{\Lambda}^t, \boldsymbol{U}^t),\end{aligned} \tag{19}$$

$$\begin{aligned}\hat{\boldsymbol{Y}}_{1\_\mathrm{sub}}^{t+1} = \frac{1}{2\rho+1}(&\boldsymbol{Y}_{1\_\mathrm{sub}} + \rho\boldsymbol{U}_{P\times N_{\mathrm{sym}}}^t + 2(\boldsymbol{\Lambda}_{N_{\mathrm{sym}}\times P}^t)^{\mathrm{H}} +\\ &\rho(\boldsymbol{U}_{N_{\mathrm{sym}}\times P}^t)^{\mathrm{H}}),\end{aligned} \tag{20}$$

$$\boldsymbol{\Phi}^{t+1} = \frac{1}{2}\boldsymbol{U}_{P\times P}^t + \frac{1}{2}(\boldsymbol{U}_{P\times P}^t)^{\mathrm{H}} + \frac{1}{\rho}(\boldsymbol{U}_{P\times P}^t - \frac{\tau}{2}\boldsymbol{I}_{P\times P}), \tag{21}$$

$$\boldsymbol{u}^{t+1} = \frac{1}{\rho}\boldsymbol{\Gamma}\mathrm{conj}(g(\boldsymbol{\Lambda}_{N_{\mathrm{sym}}\times N_{\mathrm{sym}}}^t) + \rho g(\boldsymbol{U}_{N_{\mathrm{sym}}\times N_{\mathrm{sym}}}^t) - \frac{\tau}{2}\boldsymbol{e}_1), \tag{22}$$

$$\boldsymbol{U}^{t+1} = \arg\min_{\succeq 0} L(\hat{\boldsymbol{Y}}_{1\_\mathrm{sub}}^{t+1}, \boldsymbol{u}^{t+1}, \boldsymbol{\Phi}^{t+1}, \boldsymbol{\Lambda}^t, \boldsymbol{U}^t), \tag{23}$$

$$\boldsymbol{\Lambda}^{t+1} = \boldsymbol{\Lambda}^t + \rho\left(\boldsymbol{U}^{t+1} - \begin{bmatrix}\boldsymbol{\Phi}^{t+1} & \hat{\boldsymbol{Y}}_{1\_\mathrm{sub}}^{t+1}\\ (\hat{\boldsymbol{Y}}_{1\_\mathrm{sub}}^{t+1})^{\mathrm{H}} & \boldsymbol{T}(\boldsymbol{u})\end{bmatrix}\right), \tag{24}$$

where the superscript t represents the tth iteration; conj$(\cdot)$ means taking conjugate for each element of the input matrix; $\boldsymbol{I}_{p\times p}$ is a $p\times p$ indenfity matrix; $\boldsymbol{a}=g(\boldsymbol{A})$ indicates that the matrix $\boldsymbol{A}$ is converted into a vector $\boldsymbol{a}$, and $\boldsymbol{a}_i=\mathrm{sum}(\boldsymbol{A}_{p,q}|q-p+1=i)$; $\boldsymbol{e}_1$ is the first column vector of the identity matrix; $\boldsymbol{\Gamma}=\mathrm{diag}(1/N_{\mathrm{sym}},1/N_{\mathrm{sym}}-1,\cdots,1)$; $\hat{\boldsymbol{Y}}_{1\_\mathrm{sub}}$ can be obtained after iterative convergence. Finally, to obtain the Doppler parameter estimation of targets, the dual solution method in [21] is used to search the peak for each row of $\hat{\boldsymbol{Y}}_{1\_\mathrm{sub}}$.

3.3 Delay parameters estimation

After obtaining the accurate estimation of the Doppler frequency of targets, the RSC method is proposed to estimate their delay with high precision. Firstly, a known delay vector $\boldsymbol{\tau}_{\mathrm{offset}}$ is compensated on the reference signal, and the compensated signal in the mth OFDM symbol, the signal in the nth subcarrier can be expressed as

$$f_m^l[n]=s_m[n]\exp(\mathrm{j}2\pi\boldsymbol{\tau}_{\mathrm{offset}}(l)f_n),\ \ l=1,2,\cdots,L \tag{25}$$

where the l is the delay vector index. The delay vector can be expressed as $\boldsymbol{\tau}_{\mathrm{offset}}=[(L-1)/L,(L-2)/L,\cdots,0]^{\mathrm{T}}$, and L is equivalent to the sampling multiple.

Let $\boldsymbol{F}_{\mathrm{offset}}$ be a three-dimensional (3D) matrix after RSC, and the structure is shown in Fig. 2. The matrix of the shaded part in Fig. 2 is represented as $\boldsymbol{F}_{\mathrm{offset}}(:,\ :,\ l)$ whose (n,m)th element is $f_m^l[n]$ in the lth layer matrix of $\boldsymbol{F}_{\mathrm{offset}}$.

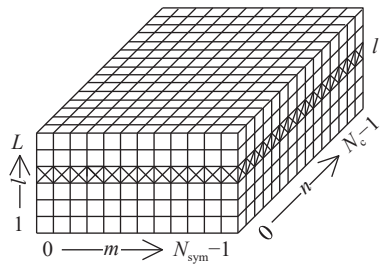

Fig. 2 Structure of the matrix $\boldsymbol{F}_{\mathrm{offset}}$

Let $\hat{\boldsymbol{D}}\in\mathbf{C}^{N_{\mathrm{c}}\times N_{\mathrm{sym}}\times L}$ be a new matrix with its entries the element-wise division of the received symbols $r_m[n]$ and compensated reference symbols $f_m^l[n]$, given as

$$\hat{D}_m^l[n]=\frac{r_m[n]}{f_m^l[n]},\ \ l=1,2,\cdots,L. \tag{26}$$

Therefore, the influence of Doppler parameters should be eliminated firstly, performing DFT on the Doppler dimension. Formally, DFT is performed on each row in each layer of the 3D matrix $\hat{\boldsymbol{D}}$, one has

$$\hat{\boldsymbol{D}}_1(:,\ :,\ l)=\ \hat{\boldsymbol{D}}(:,\ :,\ l)\boldsymbol{F}_{N_{\mathrm{sym}}},\ \ l=1,2,\cdots,L. \tag{27}$$

Then, performing IDFT on each column of the matrix $\hat{\boldsymbol{D}}_1(:,\ :,\ l)$ in (27), one has

$$\hat{\boldsymbol{D}}_2(:,\ :,\ l)=\boldsymbol{F}_{N_{\mathrm{c}}}^{\mathrm{H}}\hat{\boldsymbol{D}}_1(:,\ :,\ l). \tag{28}$$

The resulting matrix is $\hat{\boldsymbol{D}}_2\in\mathbf{C}^{N_{\mathrm{c}}\times N_{\mathrm{sym}}\times L}$, to speed up processing time and reduce the storage memory, we set $L=10$ and extend five delay bins forward and backward respectively based on the rough estimated delay. For example, the rough estimated delay is g_τ^p of the target p, then the range of delay fine estimation is taken as $[g_\tau^p-5,\ g_\tau^p+5]$ $(5\leqslant g_\tau^p\leqslant N_{\mathrm{c}}-6)$. The signal to be estimated of the pth target can be expressed as

$$\hat{\boldsymbol{D}}_2([g_\tau^p-5,\ g_\tau^p+5],\ g_f^p,\ :)\in\mathbf{C}^{11\times1\times10}. \tag{29}$$

Then the compensated signal of the pth target can be expressed as

$$\boldsymbol{d}_p=\mathrm{reshape}((\hat{\boldsymbol{D}}_2([g_\tau^p-5,\ g_\tau^p+5],\ g_f^p,\ :)^{\mathrm{T}}),\ [\cdot],\ 1)\in\mathbf{C}^{110\times1} \tag{30}$$

where reshape$(\cdot,\ [\cdot],\ 1)$ means converting the matrix into a column vector. Finally, the accurate delay estimation is found in vector $\boldsymbol{d}_p$.

To emphasize the effectiveness of RSC, Fig. 3 gives the delay dimension signal after compensation by RSC, which contains two adjacent delay targets $(g_\tau^{p_1}=51.2,\ g_\tau^{p_2}=52)$. As shown in Fig. 3, the compensated signal obtained by RSC has the following two advantages: (i) the peak value is closer to the real value, and the amplitude of target estimation is increased accordingly; (ii) it has potential advantages in near-neighbor target recognition. These illustrate the necessity of the RSC method for target time delay estimation in passive radar.

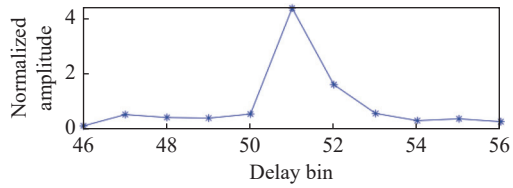

(a) Delay dimension obtained by MSD

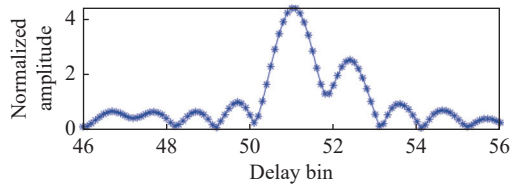

(b) Delay dimension after compensation by RCS

Fig. 3 Comparison of uncompensated and RSC compensated signals in delay dimension

4. Simulation analysis

In this section, we evaluate the coarse-fine joint estimation method based on AN-RSC using metrics of root

mean square error (RMSE) of target parameter and computational complexity.

4.1 Simulation setup

To verify the effectiveness of the proposed method, one illuminator transmits the 4 quadrature amplitude modulation (4QAM)-modulated OFDM signal in the simulations, which contains two parts, namely the frame header (420 symbols) and frame body (3 780 symbols). The baseband sampling rate (equal bandwidth sampling) is 7.56 MHz. 180 OFDM blocks for signal processing are used, namely approximately 0.1 s coherent processing interval. The three targets are assumed to be point scatterers in our simulations, and the values of the simulation parameters are listed in Table 1.

Table 1 Simulation parameters (input SNR: SNR_i)

Parameter	Target 1	Target 2	Target 3
Delay bin	50.55	102.93	155.36
Doppler shift/Hz	−106.23	−59.36	105.45
SNR_i/dB	−30	−25	−15

Fig. 4(a)−Fig. 4(c) present the Doppler shifts estimation for three simulation objectives in Table 1 by MSD, MMV-AN, optimized-MUSIC (OP-MUSIC) [29], extended OMP (EOMP) [14], and RSC methods. One can see that as the target input SNR increases, the estimation results of these algorithms are closer to the true Doppler position of the target. Compared with the MSD method, the Doppler estimation accuracy of these methods is improved, which proves the correctness of these algorithms. From Fig. 4(a)−Fig. 4(c), compared with the OP-MUSIC and EOMP algorithm, the estimated values of the MMV-AN and RSC are all closer to the real position of the target, which proves the performance of the algorithm in estimation accuracy.

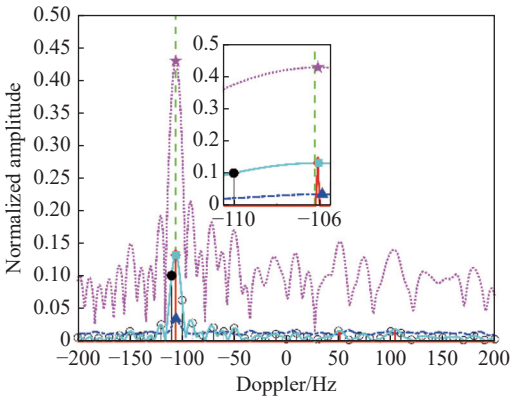

(a) Target 1 (Delay bin=51, SNR_i=−30 dB)

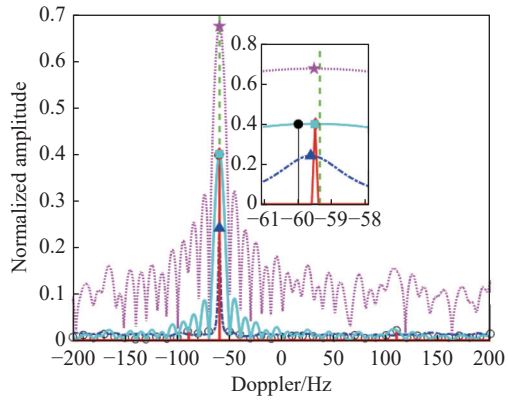

(b) Target 2 (Delay bin=103, SNR_i=−25 dB)

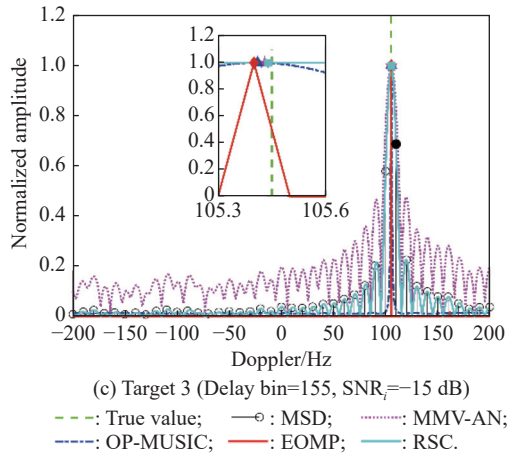

(c) Target 3 (Delay bin=155, SNR_i=−15 dB)

Fig. 4 High precision Doppler estimation of three targets in Table 1 using different methods

Fig. 5 gives the simulation results for high accuracy estimation of delay by MSD, MMV-AN, OP-MUSIC, EOMP, and RSC methods. Due to the block processing of the signal, the signal SNR loss, and the input SNR of Target 1 is as low as −30 dB, which results in incorrect time delay estimation by the OP-MUSIC algorithm in Fig. 5(a). In Fig. 5(c), the value of delay estimation of the OP-MUSIC algorithm is close to the true value of delay of Target 3. These prove that the estimation accuracy of the OP-MUSIC algorithm is affected by the SNR of the signal. Compared with the OP-MUSIC algorithm, the EOMP algorithm still has better estimation results in a low SNR environment. During the simulation, it is found that the estimation accuracy of the EOMP algorithm increases with the increase of the grid density, but the targets are split into many scatterers once the coherence of the sensing matrix increases, which may get a false target position. From Fig. 5(a)−Fig. 5(c), compared with the AN, OP-MUSIC, and EOMP algorithms, the estimated value of the RSC method is closest to the real position of the target, and the amplitude of the target estimation is improved compared with the MSD method, which benefits target detection.

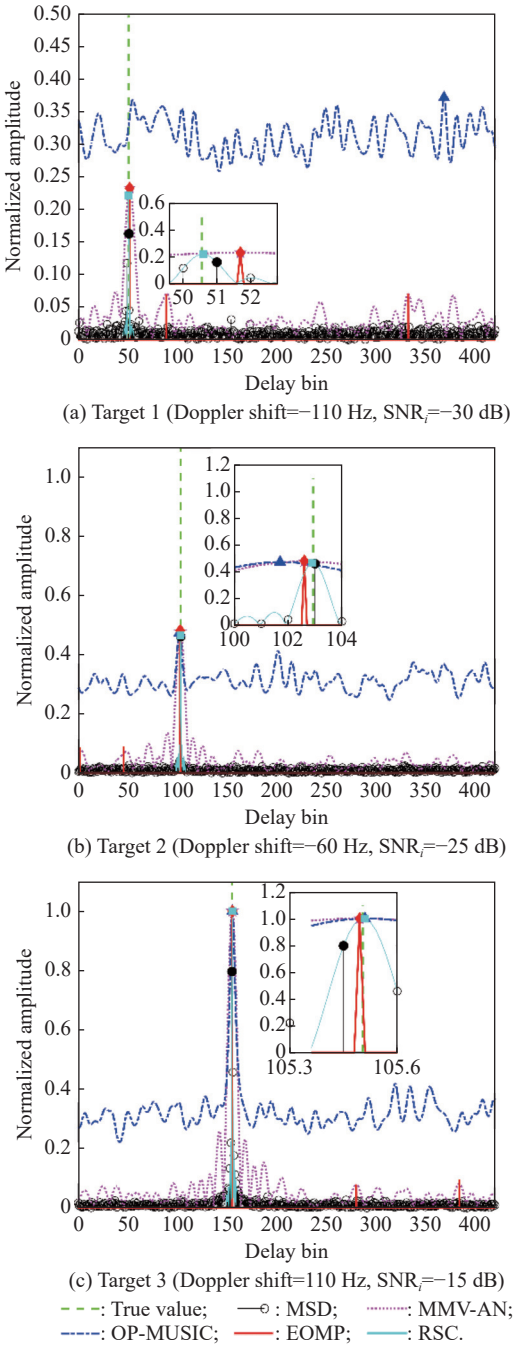

Fig. 5 High precision delay estimation of three targets in Table 1 using different methods

Table 2 lists the values of parameter estimation using different methods. As can be seen from the Table 2, these algorithms can make the high-precision estimation of the time delay and Doppler of the target. In the Doppler dimension, the methods of MMV-AN and RSC have better estimation accuracy than other algorithms. In the delay dimension, the proposed RSC method has better performance despite the low SNR compared to other algorithms.

Table 2 Parameter estimation of different methods

Parameter	Method	Target 1	Target 2	Target 3
Doppler shift/Hz	True value	−106.23	−59.36	105.45
	MSD	−110	−60	110
	MMV-AN	−106.09	−59.53	105.43
	OP-MUSIC	−105.89	−58.63	105.41
	EOMP	−106.1	−59.5	105.4
	RSC	−106.07	−59.52	105.44
Delay bin	True value	50.55	102.93	155.36
	MSD	51	103	155
	MMV-AN	51.7	102.6	155.3
	OP-MUSIC	368.4	101.7	155.4
	EOMP	51.7	102.6	155.3
	RSC	50.6	102.9	155.4

In order to evaluate the performance of the proposed method and others, the off-grid values of delay and Doppler are uniformly distributed within [−0.5,0.5], and the input SNR varies from −35 dB to 0 dB with a step of 5 dB. For each SNR value, 2 000 Monte Carlo (MC) simulations are performed with independently generated measurements. The RMSEs of the delay-Doppler are utilized to evaluate the performance. The delay RMSE and Doppler RMSE are defined as

$$\text{delay\_RMSE}_i^q = \sqrt{\frac{1}{M_c}\sum_{m=1}^{M_c}\left(t_i^q - \hat{t}_{i,m}^q\right)^2}, \tag{31}$$

$$\text{Doppler\_RMSE}_i^q = \sqrt{\frac{1}{M_c}\sum_{m=1}^{M_c}\left(f_i^q - \hat{f}_{i,m}^q\right)^2}, \tag{32}$$

where $\hat{t}_{i,m}^q$ and $\hat{f}_{i,m}^q$ denote the delay and Doppler estimates of the qth target at scan i in the mth MC run; t_i^q and f_i^q denote the true values of the delay and Doppler estimates of the qth target at scan i. In this paper, we randomly generate a target so that $q = 1$. $M_c = 2\,000$ represents the number of MC simulations.

The RMSEs using different estimation methods under different SNR conditions are shown in Fig. 6. Fig. 6(a) and Fig. 6(b) show the delay RMSE and Doppler RMSE of the different SNR conditions, respectively. As shown in Fig. 6(a), the performance of the OP-MUSIC algorithm is easily affected by SNR. When the input SNR of the signal is greater than −30 dB, the estimation accuracy of the MMV-AN, OP-MUSIC, EOMP, and RSC methods is higher than that of the MSD method, which can

be used for fine estimation. Because the estimation accuracy of the signal is mainly affected by SNR and grid density, when the grid is sparse, the estimation accuracy is mainly affected by grid density. When the grid density is large enough, SNR is the main factor of accuracy. Therefore, the estimation accuracy of MSD remains almost unchanged. Compared with the OP-MUSIC, EOMP algorithms, the Doppler RMSEs of MMV-AN and RSC methods are lower, and they are close to the Cramer-Rao bounds (CRBs). Compared with the RSC method, when SNR < −15 dB, the accuracy of MMV-AN is equivalent to that of RSC. When the SNR is large enough, the estimation accuracy of MMV-AN is higher, and the accuracy of RSC tends to the grid density boundary. As shown in Fig. 6 (b), compared with other methods, the RSC method has the highest accuracy and stable robustness in delay estimation. The delay estimation accuracy of MMV-AN and OP-MUSIC algorithms is easily affected by signal noise, while the delay RMSEs of EOMP, MSD, and RSC methods remain basically unchanged. Due to the coherence of the sensing matrix, the estimation accuracy of the EOMP algorithm is limited. The accuracy of MSD and RSC methods is mainly related to the grid density, and the MSD is a special form of RSC (i.e., no signal compensation, compensation step $L = 0$). By increasing the step size, the estimation accuracy of the RSC method is greatly improved. In addition, in the simulations, the search accuracy of all algorithms is set to 0.1 delay unit, which results in the accuracy of these algorithms being limited by the grid density and not close to the CRB. It should be noted that increasing the search accuracy of the algorithm can improve the estimation accuracy, which is closer to CRB, but it also greatly increases the computational complexity of the algorithm.

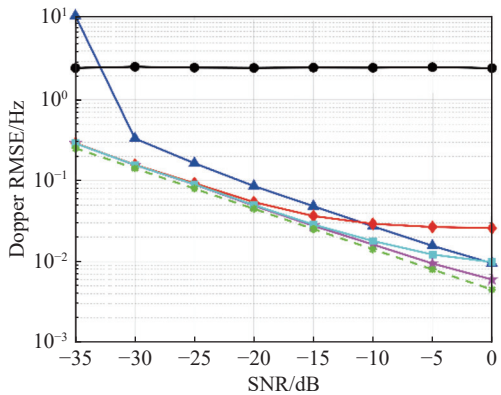

(a) Doppler RMSE versus SNR

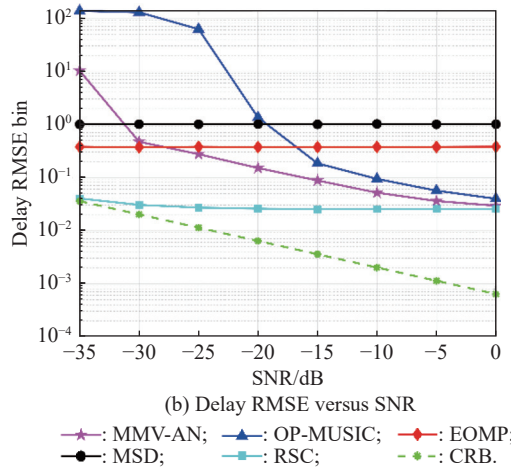

(b) Delay RMSE versus SNR

Fig. 6 2 000 MC simulation results for each SNR

4.2 Computational complexity

The computational complexities of the method for obtaining parameter estimates come from the following four stages: signals conversion from the time domain to the symbol domain, OFDM channel response estimation, target Doppler dimension estimation, and target delay dimension estimation. The first two stages of these methods are exactly the same, except for the third and fourth stages. Therefore, only the complexity analysis of parameter estimation is considered below.

The computational complexity of 2D-AN [21,30] is mainly reflected in two aspects: one is to solve the SDP via the ADMM, which requires $O((N_{\mathrm{c}}N_{\mathrm{sym}})^3)$; the other is to jointly estimate the delay and Doppler parameters of targets by dual solution, which requires $O(N_f N_\tau N_{\mathrm{c}} N_{\mathrm{sym}})$, where N_f and N_τ are the number of Doppler and delay grids respectively. In this paper, the computational complexity of the coarse-fine joint estimation method is mainly reflected in three aspects: the coarse estimation of target parameters using (8) and (9), estimation of target Doppler parameters, and estimation of target delay parameters. Firstly, the coarse estimation of target parameters requires $O(N_{\mathrm{c}}N_{\mathrm{sym}}(\log_2(N_{\mathrm{sym}})+\log_2(N_{\mathrm{c}})))$. Then, the MMV-AN, EOMP, OP-MUSIC, and RSC methods are used to estimate the Doppler parameters respectively, and computational complexity as follows: $O((N_{\mathrm{sym}}+P)^3)+O(PN_fN_{\mathrm{sym}})$, $O(N_fN_{\mathrm{sym}})+O(PG_fN_fN_{\mathrm{sym}})$, $O(PN_{\mathrm{sym}}^2)+O(2PN_{\mathrm{sym}}^3)+O(PN_f(2N_{\mathrm{sym}}(N_{\mathrm{sym}}-K_f)+N_{\mathrm{sym}}))$, and $O(2L_fN_{\mathrm{c}}N_{\mathrm{sym}}(1+\log_2(N_{\mathrm{sym}})+0.5\log_2(N_{\mathrm{c}})))$, where G_f is the number of iterations, K_f represents the number of frequency sources， and L_f is equivalent to the sampling multiple in Doppler domain. Finally, the parameter estimation of the delay dimension with MMV-AN, EOMP, OP-MUSIC, and RSC methods, respectively. It is not diffi-

cult to find that the complexity of the delay dimension of MMV-AN, EOMP, OP-MUSIC, and RSC methods are basically the same as the complexity expression of the Doppler dimension, except that the value of dimension and grid is different. The computational complexity of the RSC method requires $O(L_\tau N_c N_{sym}\log_2(N_c)) + O(2L_\tau N_c N_{sym}\cdot(\log_2(N_c N_{sym}) + \log_2(N_{sym})))$, which is related to the value of L and coarse estimation. The overall computational complexities of the different methods of solving the third and fourth stages are concluded in Table 3.

Table 3 Comparison of the computational complexity of different methods

Parameters to be estimated	Method	Computational cost
Delay and Doppler	2D-AN	$O((N_c N_{sym})^3 + N_f N_\tau N_c N_{sym})$
	MSD	$O(N_c N_{sym}(\log_2(N_{sym}) + \log_2(N_c)))$
Delay	RSC	$O(2L_\tau N_c N_{sym}(\log_2(N_c N_{sym}) + \log_2(N_{sym}) + 0.5\log_2(N_c)))$
	MMV-AN	$O((N_c + P)^3 + PN_\tau N_c)$
	EOMP	$O(N_\tau N_c + PG_\tau N_\tau N_c)$
	OP-MUSIC	$O(PN_c^2 + 2PN_c^3 + PN_\tau(2N_c(N_c - K_\tau) + N_c))$
Doppler	RSC	$O(2L_f N_c N_{sym}(1 + \log_2(N_{sym}) + 0.5\log_2(N_c)))$
	MMV-AN	$O((N_{sym} + P)^3 + PN_f N_{sym})$
	EOMP	$O(N_f N_{sym} + PG_f N_f N_{sym})$
	OP-MUSIC	$O(PN_{sym}^2 + 2PN_{sym}^3 + PN_f(2N_{sym}(N_{sym} - K_f) + N_{sym}))$

An intuitive comparison for computational complexity is given via a study case. Assume that $N_c = 3\,780$ and $N_{sym} = 180$ and that the parameter configuration for the AN-RSC is $P = 1$, $G = 3$, $N_f = 1.8\times10^5$, $L_f = 1\,000$, and $L_\tau = 10$. The computational complexity of the coarse-fine joint method based on AN-RSC is $4.979\,9\times10^8$. For comparison, the computational complexity of the 2D-AN algorithm is $3.155\,0\times10^{17}$, and its parameter configuration $N_\tau = 4\,200$.

It can be concluded that the complexity of the coarse-fine joint estimation method is lower than that of 2D-AN. In the Doppler estimation dimension, the complexity of MMV-AN is $3.833\,0\times10^7$. The complexity of OP-MUSIC is $1.164\,3\times10^{10}$ with its parameter configuration $K_f = 1$. Due to the coherence of the sensing matrix, the grid size of the EOMP algorithm is limited, and the parameter configuration for the EOMP is $N_f = 1.8\times10^4$, and $G_f = G_\tau = 3$. So, the complexity of EOMP is $1.296\,0\times10^7$, and that of RSC is $1.964\,2\times10^{10}$. It can be seen that the complexity of RSC is the largest. Therefore, compared with the RSC method, the MMV-AN algorithm is more suitable for Doppler estimation. In the delay estimation dimension, the complexity of MMV-AN, EOMP, OP-MUSIC and RSC are $5.406\,9\times10^{10}$, $6.350\,4\times10^7$, $1.740\,3\times10^{11}$, and $4.464\,8\times10^8$. It can be seen that the algorithm complexity of EOMP is the smallest, OP-MUSIC is the largest, and RSC is close to EOMP. Thus, the coarse-fine joint estimation method based on AN-RSC is attractive in computational load for real-time implementation.

5. Conclusions

In this paper, the delay and Doppler of targets in OFDM-based passive radar are investigated. In order to reduce the complexity of joint estimation parameters, we have proposed a coarse-fine joint estimation method, in which the MMV-AN is used to perform sparse reconstruction of Doppler dimension, and then, the RSC method is used to perform sparse reconstruction of range dimension. Compared to previous OP-MUSIC and EOMP algorithms, we can achieve high-precision parameter estimation of the target scenario and do not suffer from the heavy computational burden. The effectiveness of the proposed method is verified by simulated data. In future work, the influence of adjacent targets on their parameter estimation will be taken into consideration. The high resolution of adjacent targets using the OFDM-based passive radar system is also an interesting topic.

References

[1] HADI M A, TABASSUM M N, ALSHEBEILI S. Compressive sensing based high-resolution passive bistatic radar. Signal, Image and Video Processing, 2017, 11(4): 635–642.

[2] CAO X M, YI J X, GONG Z P, et al. Data fusion of target characteristic in multistatic passive radar. Journal of Systems Engineering and Electronics, 2021, 32(4): 811–821.

[3] FILIP-DHAUBHADEL A, SHUTIN D. Long coherent integration in passive radar systems using super-resolution sparse bayesian learning. IEEE Trans. on Aerospace and Electronic Systems, 2021, 57(1): 554–572.

[4] COLEMAN C, YARDLEY H. Passive bistatic radar based on target illuminations by digital audio broadcasting. IET Radar, Sonar & Navigation, 2008, 2(5): 366–375.

[5] PALMER J E, HARMS H A, SEARLE S J, et al. DVB-T passive radar signal processing. IEEE Trans. on Signal Processing, 2013, 61(8): 2116–2126.
[6] National Radio and Television Administration. Framing structure, channel coding and modulation for digital television terrestrial broadcasting systems. Chinese National Standard GB 20600-2006, 2006. (in Chinese)
[7] STURM C, WIESBECK W. Waveform design and signal processing aspects for fusion of wireless communications and radar sensing. Proceedings of the IEEE, 2011, 99(7): 1236–1259.
[8] YADAV S K, GEORGE N V. Coarray MUSIC-group delay: high-resolution source localization using non-uniform arrays. IEEE Trans. on Vehicular Technology, 2021, 70(9): 9597–9601.
[9] LI P, LI J F, ZHAO G F. Low complexity DOA estimation for massive UCA with single snapshot. Journal of Systems Engineering and Electronics, 2022, 33(1): 22–27.
[10] WANG Y F, HU B, ZHANG L X, et al. Unitary NSF method for monostatic MIMO radar with non-orthogonal waveforms. Circuits, Systems, and Signal Processing, 2022, 41(5): 2963–2976.
[11] WEN J F, YI J X, WAN X R, et al. DOA estimation based on multi-frequency joint sparse Bayesian learning for passive radar. Journal of Systems Engineering and Electronics, 2022, 33(5): 1052–1063.
[12] YANG T Y, ZHENG J B, SU T, et al. Fast and robust super-resolution DOA estimation for UAV swarms. Signal Processing, 2021, 188: 108187.
[13] FRADY E P, KLEYKO D, SOMMER F T. Variable binding for sparse distributed representations: theory and applications. IEEE Trans. on Neural Networks and Learning Systems, 2023, 34(5): 2191−2204.
[14] GONG P C, WANG W Q, LI F C, et al. Sparsity-aware transmit beamspace design for FDA-MIMO radar. Signal Processing, 2018, 144: 99–103.
[15] DEMISSIE B, BERGER C R. High-resolution range-Doppler processing by coherent block-sparse estimation. IEEE Trans. on Aerospace and Electronic Systems, 2014, 50(2): 843–857.
[16] FENG W K, FRIEDT J M, CHERNIAK G, et al. Batch compressive sensing for passive radar range-Doppler map generation. IEEE Trans. on Aerospace and Electronic Systems, 2019, 55(6): 3090–3102.
[17] BAI X, GUO H J, ZHAO J, et al. Compressed Sensing-based range-doppler processing method for passive radar. Wireless Communications and Mobile Computing, 2021, 2021: 5570498.
[18] CHI Y J, SCHARF L L, PEZESHKI A, et al. Sensitivity to basis mismatch in compressed sensing. IEEE Trans. on Signal Processing, 2011, 59(5): 2182–2195.
[19] TANG G G, BHASKAR B N, SHAH P, et al. Compressed sensing off the grid. IEEE Trans. on Information Theory, 2013, 59(11): 7465–7490.
[20] SULIMAN M A, DAI W. Mathematical theory of atomic norm denoising in blind two-dimensional super-resolution. IEEE Trans. on Signal Processing, 2021, 69: 1681–1696.
[21] ZHENG L, WANG X D. Super-resolution delay-Doppler estimation for OFDM passive radar. IEEE Trans. on Signal Processing, 2017, 65(9): 2197–2210.
[22] SONG L, GE Z, LAM E Y. Dual alternating direction method of multipliers for inverse imaging. IEEE Trans. on Image Processing, 2022, 31: 3295–3308.
[23] LAN L, ROSAMILIA M, AUBRY A, et al. Single-snapshot angle and incremental range estimation for FDA-MIMO radar. IEEE Trans. on Aerospace and Electronic Systems, 2021, 57(6): 3705–3718.
[24] YANG Z, XIE L H. Continuous compressed sensing with a single or multiple measurement vectors. Proc. of the IEEE Workshop on Statistical Signal Processing, 2014: 308–311.
[25] WEN J F, YI J X, WAN X R. Sparse representation for target parameter estimation in CDR-based passive radar. IEEE Geoscience and Remote Sensing Letters, 2020, 18(6): 1024–1028.
[26] KONG B, WANG Y H, LEUNG H, et al. Sparse representation based range-doppler processing for integrated OFDM radar communication networks. International Journal of Antennas and Propagation, 2017, 2017(10): 6528956.
[27] STURM J F. Using SeDuMi 1.02, a MATLAB toolbox for optimization over symmetric cones. Optimization Methods and Software, 1999, 11(1/4): 625–653.
[28] TOH K C, TODD M J, TTNC R H. SDPT3-a MATLAB software package for semidefinite programming, version 1.3. Optimization Methods and Software, 1999, 11(1/4): 545–581.
[29] FARSHOUH M, SRAR J, MANSOUR A. Angle of arrival estimation using OP-MUSIC algorithm for both coherent and non-coherent sources. Proc. of the Security & Protection of Information Conference, 2021. https://www.researchgate.net/publication/355228557.
[30] ZHANG T, CUO J C, LAI R. Gridless sparse recovery for non-sidelooking space-time adaptive processing based on atomic norm minimization. Journal of Electronics & Information Technology, 2021, 43(5): 1235−1242. (in Chinese)

Biographies

WANG Chujun was born in 1991. She received her B.E. degree in electronic and information engineering from the College of Technology, Hubei Engineering University in 2015. She received her M.S. degree in information and communication engineering from Chongqing University of Posts and Telecommunications in 2018. She is working toward her Ph.D. degree at the School of Electronic Information, Wuhan University. Her research interests are passive radar signal processing and array signal processing.
E-mail: 2019182120077@whu.edu.cn

WAN Xianrong was born in 1975. He received his B.E. degree in electrical and electronic engineering from former Wuhan Technical University of Surveying and Mapping, Wuhan, China, in 1997, and Ph.D. degree from Wuhan University, Wuhan, in 2005. He is now a professor and Ph.D. candidate supervisor of the School of Electronic Information, Wuhan University. Recent years he has hosted and participated in more than ten national research projects, and published more than 150 academic papers. His main research interests include design of new radar system such as passive radar, over-the-horizon radar, and array signal processing.
E-mail: xrwan@whu.edu.cn

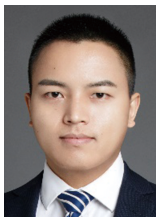

YI Jianxin was born in 1989. He received his B.E. degree in electrical and electronic engineering, and Ph.D. degree in radio physics, from Wuhan University, Wuhan, China, in 2011 and 2016, respectively. He is now an associate professor with the School of Electronic Information, Wuhan University. He was a recipient of the 2017 Excellent Doctoral Dissertation Award of the Chinese Institute of Electronics. He has been supported by the Postdoctoral Innovation Talent Support Program of China. His main research interests include radar signal processing, target tracking, and information fusion.
E-mail: jxyi@whu.edu.cn

CHENG Feng was born in 1975. He received his Ph.D degree in radion physics from Wuhan University, Wuhan, in 2006. He is currently an associate professor with Wuhan University. His main research interests include radar signal processing, radio ocean remote sensing, and radar software engineering.
E-mail: cwing@whu.edu.cn